Optics and Lasers in Engineering 185 (2025) 108721

Contents lists available at ScienceDirect

Optics and Lasers in Engineering

journal homepage: www.elsevier.com/locate/optlaseng

Layered phase restoration method for dual-wavelength digital holographic microscopy based on linear programming

Yuxuan Zhao [a], Lei Zeng [a], Zhiming Lin [a], Qiwen Jin [a], Yingchun Wu [a], Chenghang Zheng [a], Zhibin Wang [b], Yongxin Zhang [c], Xuecheng Wu [a,c,*]

[a] State Key Laboratory of Clean Energy Utilization, Zhejiang University, Hangzhou 310027, China
[b] College of Environmental & Resource Sciences, Zhejiang University, Hangzhou 310058, China
[c] Jiaxing Research Institute, Zhejiang University, Jiaxing 314000, China

ARTICLE INFO

Keywords:
Dual-wavelength digital holographic microscopy
Topographic measurement
Micro-nano structure
Phase restoration

ABSTRACT

Dual-wavelength digital holographic microscopy is a method to acquire surface topography of high-depth samples, offering a broader depth range compared to single-wavelength technique. When applying to high aspect ratio structures, however, optical aberrations are difficult to remove, resulting in phase restoration distortions. To address this limitation, we developed a layered phase restoration method for DW-DHM. This approach restores the phase by decomposing the step structure into layers and applying a targeted de-aberration process at each layer, followed by precise dual-wavelength phase unwrapping through linear programming algorithm (LPA). Simulations and experimental results show that, while preserving the noise robustness of LPA, the proposed method provides significantly enhanced resistance to various aberrations. For topographic measurements of complex micro-nano scale step structures, this approach effectively mitigates the issue in LPA where the phase restoration affected by hard-to-eliminate aberrations, demonstrating its potential for advanced applications in micro-nano device measurement.

1. Introduction

Digital holographic microscopy (DHM), a combination of micro-imaging and digital holography, represents a phase-imaging technique renowned for its non-contact nature and delivery of high-quality, high-resolution images. Based on the principle of holography proposed by Dennis Gabor in 1948 [1], DHM works by recording the amplitude and phase information of objects' waves through the phenomenon of light interference and reconstructing a three-dimensional image of the sample using the theory of light diffraction. It stands out as one of the most suitable approaches for precise topographic measurements of micro-structures [2,3]. Dual-wavelength holographic microscopy (DW-DHM) is an extension of single-wavelength holographic microscopy (SW-DHM), aiming to extend the longitudinal measurement range of DHM in microscopic morphology [4,5]. The concept of employing multiple wavelengths to extend measurement ranges beyond a single wavelength was first proposed by Michelson and Benoit in 1894 [6], with Wyant achieving the initial application of multi-wavelength techniques in holography in 1971 [7]. In recent years, DW-DHM has evolved into an important method for augmenting longitudinal measurement ranges [8–11]. The associated technology has also been sufficiently developed. Conventional DWDH uses two cameras [12] or two separate experiments to record the holograms of two wavelengths. In recent years, through the arrangement of optical elements such as polarizing mirrors [13], it was possible to obtain two-wavelength holograms with just one camera exposure. In the latest research, a Wollaston prism(WP) was used to separate the two orthogonal-polarized reference beams of two different wavelengths [14].

In the field of micro-nano device processing, surface topography characteristics are important parameters for evaluating the manufacturing quality and performance of micro-nano structures. It is closely related to the service life and physical & mechanical properties of the chips [15]. MEMS (Micro-Electro-Mechanical System) chips, as the most representative micro-nano structured devices, have advanced to 30:1 high aspect ratio microgroove structures [16,17]. For step structure measurements in micro-nano devices, SW-DHM cannot unambiguously

* Corresponding author at: State Key Laboratory of Clean Energy Utilization, Zhejiang University, Hangzhou 310027, China.
E-mail address: wuxch@zju.edu.cn (X. Wu).

https://doi.org/10.1016/j.optlaseng.2024.108721
Received 1 August 2024; Received in revised form 6 November 2024; Accepted 22 November 2024
Available online 28 November 2024

determine the interferometric orders of holograms [18]. The phase unwrapping algorithms fail to identify large steps optically thicker than the illumination wavelength, due to the surface non-continuous variation of the steps. This limitation leads to measurement inaccuracy of SW-DHM technique. In comparison, DW-DHM systems are capable of observing MEMS topography within the scale range of 1 to 50 μm and can determine deformations in intricate structures [13,19]. While dual-wavelength holography expands the range of height detection, it also introduces a proportional increase in measurement standard deviation [20]. Consequently, a critical concern in DW-DHM revolved around achieving high-precision shape restoration. In the current research, the primary dual-wavelength phase restoration algorithms mainly include direct phase subtraction and linear programming methods. The direct phase subtraction method derives a continuous phase distribution by directly subtracting two single-wavelength phases and compensating 2π for phase discrepancies when the subtraction yields negative values [21]. However, the accuracy of this approach is susceptible to anomalous phase jumps induced by system and measurement noise, leading to potential failure. The linear programming phase restoration method (LPA) was firstly proposed by Khmaladze et al. in 2011 [22]. Based on the linear programming, it adjusts the positions where dual-wavelength phase values fall below zero by adding 2π, thus compensating the phase difference. In subsequent studies, Wang et al. [23] introduced new constraints and Shan et al. [24] introduced new constraints, enhancing its efficacy and accuracy against noise. Recently, Shan et al. [25] further improved the calculation speed of the algorithm. Nontheless, the accuracy of LPA still depends on the precision of single wavelength phase measurement. For complex step structures on components such as MEMS systems, residual aberration within the step structure is difficult to extract further, which will significantly affect the accuracy of dual-wavelength unwrapping.

In this study, we proposed a layered phase restoration method for accurate dual-wavelength phase unwrapping of complex step structures. Under the premise of removing most of the system aberration, this method involved removing the complete aberration by layering the step structure and extracting the residual aberration of each layer respectively. Finally, linear programming was used to achieve accurate dual-wavelength phase unwrapping to restore the topography of the sample. Simulation in Section 3 demonstrated its high accuracy and robustness against noise. In Section 4, we applied this method to the measurement of a standard periodic step sample using a single-shot dual-wavelength holographic microscopy system to demonstrate the accuracy-enhancing effect of the method in practical measurements. Finally, we measured and characterized a MEMS sample with step structures to verify its potential for advanced applications in micro-nano device measurement.

2. Principle

2.1. Dual-wavelength digital holographic microscopy

In digital holographic topographic measurement, when light passes over the surface of sample, the difference in refractive index between the sample and the air will affect the light propagation trajectory. This will be reflected in the changes of the beam amplitude and phase information. The digital holographic recording and numerical reconstruction method can get the phase information changes related to the sample, and perform topographic measurements of the sample by restoring the phase information [26]. Digital holographic topographic measurement can be categorized into transmissive mode and reflective mode. The relationship between the phase information of sample and its thickness can be expressed respectively as [27],

Transmissive mode (on a transmissive surface):

$$h(x,y)=\frac{\varphi(x,y)}{2\pi(n_s-n_0)}\lambda, \tag{1}$$

reflective mode (on a reflective surface):

$$h(x,y)=\frac{\varphi(x,y)}{4\pi}\lambda, \tag{2}$$

where n_s and n_0 are the refractive index of sample and surrounding medium, respectively. $\varphi(x,y)$ is the phase of sample. λ is the wavelength of light source. In this study, the measurements were performed on opaque samples with reflective holographic systems.

Assuming that two light beams $k_1=\frac{2\pi}{\lambda_1}$ and $k_2=\frac{2\pi}{\lambda_2}$ irradiate the sample separately, holograms of two single wavelengths are formed and recorded by the CCD camera. Object light wave of sample and the reference wave interferes and propagates to the camera recording plane. Basis on the complex amplitude distribution of any cross-section in object light field $\mathbf{O}(x,y)$, the phase $\varphi(x,y)$ is calculated by numerical reconstruction:

$$\varphi(x,y)=\arctan\left[\frac{\mathrm{Im}(\mathbf{O}(x,y))}{\mathrm{Re}(\mathbf{O}(x,y))}\right]. \tag{3}$$

Assuming that both the illumination direction and the viewing direction are perpendicular to the phase zero plane, the relationship between object height and phase is expressed as

$$h(x,y)=\frac{\varphi_1(x,y)}{4\pi}\lambda_1=\frac{\varphi_2(x,y)}{4\pi}\lambda_2. \tag{4}$$

Then the phase maps at the two wavelengths are subtracted and expressed by the following equation:

$$\begin{aligned}\varphi_1(x,y)-\varphi_2(x,y)&=\frac{4\pi}{\lambda_1}h(x,y)-\frac{4\pi}{\lambda_2}h(x,y)\\&=4\pi\frac{h(x,y)}{\frac{\lambda_1\lambda_2}{\lambda_2-\lambda_1}},\end{aligned} \tag{5}$$

where

$$\Lambda=\frac{\lambda_1\lambda_2}{\lambda_2-\lambda_1}, \tag{6}$$

$$\Phi=\varphi_1(x,y)-\varphi_2(x,y), \tag{7}$$

where Φ is the synthetic phase, and Λ is the synthetic wavelength. Eq. (6) shows that the synthetic wavelength is larger than any single wavelength. Therefore, the phase of sample will no longer be wrapped when choosing suitable λ_1 and λ_2, and the range of axial height that can be directly measured is widened.

2.2. Algorithmic process

The process of proposed method is shown in Fig. 1. The initial step involves subtracting the main phase aberration from the original wrapped phase. Phase aberrations in holographic microscopy system are mainly tilt (the camera target surface and off-axis setup), chromatic aberration (the use of different wavelengths), spherical, and defocus (the use of microscope objective, phase curvature mismatch between object beam and reference beam, etc.). In addition, a variety of factors such as instability in the measurement environment, angular mismatch of component positions, etc. can introduce a small amount of higher-order aberration. The telecentric system, as a method of physical compensation, can correct most of the defocus aberration by adjusting the position of tube lens [28]. However, compared to numerical compensation methods, the telecentric system is unable to correct complex higher-order aberrations, and it is difficult to ensure the lens device mounting accuracy, including device co-axialization, alignment, and focusing, etc. ZPF method can correct complex aberrations and more adaptable to high-precision quantitative measurement scenarios. Therefore, the ZPF compensation method [29] is applied in this study. In the Zernike aberration model, the total system aberration can be described as a superposition of 36 orders of aberration types, which is expressed through the following equation:

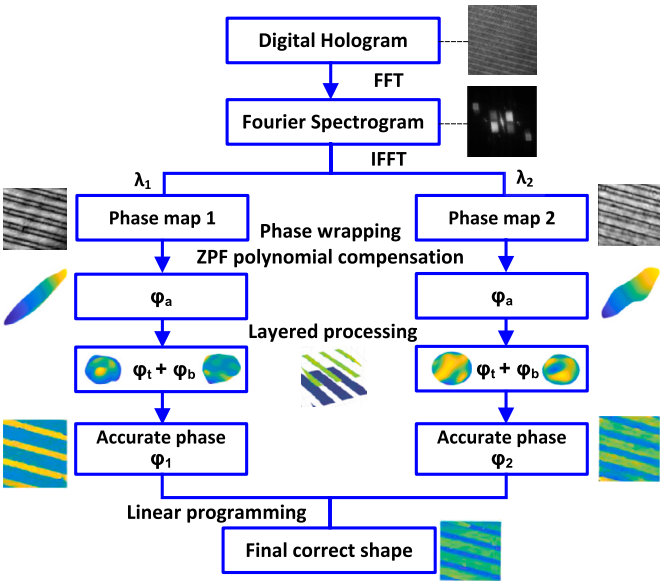

Fig. 1. Flow diagram of the proposed method.

$$\varphi_a = \begin{bmatrix} \varphi_1 \\ \varphi_2 \\ \vdots \\ \varphi_m \end{bmatrix} = \begin{bmatrix} Z_{1,0} & \cdots & Z_{1,n-1} \\ Z_{2,0} & \cdots & Z_{2,n-1} \\ \vdots & \ddots & \vdots \\ Z_{m,0} & \cdots & Z_{m,n-1} \end{bmatrix} \cdot \begin{bmatrix} a_0 \\ a_1 \\ \vdots \\ a_{n-1} \end{bmatrix}, \tag{8}$$

where m and n are the numbers of pixels on the background region and Zernike polynomial, respectively. $Z_{m,n-1}$ is the nth order of Zernike polynomial value at a pixel point, and a_{n-1} is the corresponding coefficient of phase aberration.

After initial compensation of the entire phase diagram, the step structure is layered by optimal threshold selection and the remaining aberration of the top and bottom layers are obtained respectively. Here, we employed the Otsu threshold segmentation method, the method separates the top and bottom layers by gray values μ of the image. It finds the best threshold for the whole image, splitting the gray values into two parts (top and bottom) and maximizing the class variance $\delta^2(k)$ between them. The computational process can be expressed as

$$\max[\delta^2(k)] = \max[p_t(\mu - \mu_t)^2 + p_b(\mu - \mu_b)^2], \tag{9}$$

where p_t and p_b represent the probability of corresponding pixels in the top and bottom layers, respectively. μ is the average gray value of the image, μ_t and μ_b are the average gray values for top and bottom layers, respectively. k denotes the partitioning basis for dividing top and bottom layers in gray levels.

The top and bottom layers of sample's phase are obtained after converting the gray-scale maps to original phase maps. Next, the residual aberrations of top and bottom layers are extracted by ZPF method. The residual aberrations are mainly higher-order aberrations. Then the wrapped phase φ_i with the systematic aberration removed can be expressed as

$$\varphi_i = \varphi_0 - \varphi_a - (\varphi_t + \varphi_b), \tag{10}$$

where φ_a represents the aberration obtained by Zernike polynomial fitting (Eq. (8)), typically associated with the arrangement of optical path system (e.g., microscope objective).φ_t and φ_b are the residual aberrations of the top and bottom layers after layering, respectively.

After obtaining the accurate phase diagrams of λ_1 and λ_2 through the above processes, the two single-wavelength phases, are subjected to linear programming-guided phase unwrapping [22,24]. Minor variations in height distributions obtained at different wavelengths commonly arise due to system noise, disparities in light paths at the two

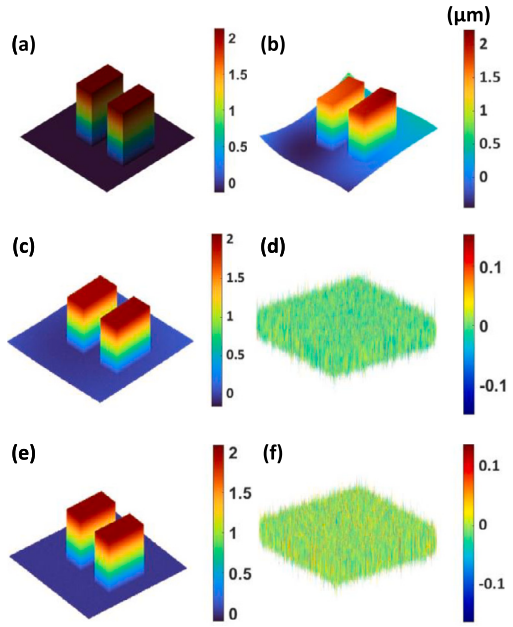

Fig. 2. Simulated results. (a) Step sample, the depth of step is 2 μm. (b) The step sample with simulated noise and aberration. (c) The height distribution calculated by LPA and (d) is the residue of the result. (e) The height distribution calculated by the proposed method and (f) is the residue graph of the result.

wavelengths, among other factors. The height distribution derived from two single-wavelength phase maps can be expressed as,

$$\begin{cases} \frac{h_1(x,y)}{\lambda_1} = \frac{1}{4\pi}\varphi_1(x,y) + m_1(x,y) \\ \frac{h_2(x,y)}{\lambda_2} = \frac{1}{4\pi}\varphi_2(x,y) + m_2(x,y), \end{cases} \tag{11}$$

where m_1 and m_2 are unknown integers at two wavelengths at pixel point (x,y), respectively. The least square value of the height difference is applied to search for the best integer matching pair of m_1 and m_2:

$$\begin{aligned} \min z &= \min\left[(h_1 - h_2)^2\right] \\ &= \min\left[\left(\frac{\varphi_1}{4\pi}\lambda_1 - \frac{\varphi_2}{4\pi}\lambda_2 + m_1\lambda_1 - m_2\lambda_2\right)^2\right]. \end{aligned} \tag{12}$$

With two parameters m_1 and m_2, the height distribution can be calculated using either of the equations in Eq. (11).

3. Numerical analysis

Numerical simulations were conducted to validate the feasibility of the proposed method. We set up a periodic step sample with a pixel size of 3.45 μm within a 560 × 560 pixel region as the measurement object. The step was set at heights of 2 μm, as shown in Fig. 2(a). The wavelengths of the laser source were chosen as λ_1 = 532 nm and λ_2 = 561 nm, respectively, resulting in a synthesized wavelength of 10.2914 μm for this setting, according to Eq. (6). Gaussian-distributed random noise was added to the sample using MATLAB (randn) function to mimic the actual conditions (Fig. 2). Additionally, the aberrations were introduced by randomly setting coefficients of order 1 to 36 in the Zernike polynomial to generate random aberrations. These simulated aberrations and noise were then applied to the simulated step sample, as depicted in Fig. 2(b).

Subsequently, we simulated the hologram formation process to obtain phase maps wrapped between -π and π at the two wavelengths. The proposed method was then applied to recover the shape of two wrapped phases. Ultimately, the accurate shape of the simulated object was successfully restored, as shown in Fig. 2(c) and (e). To further

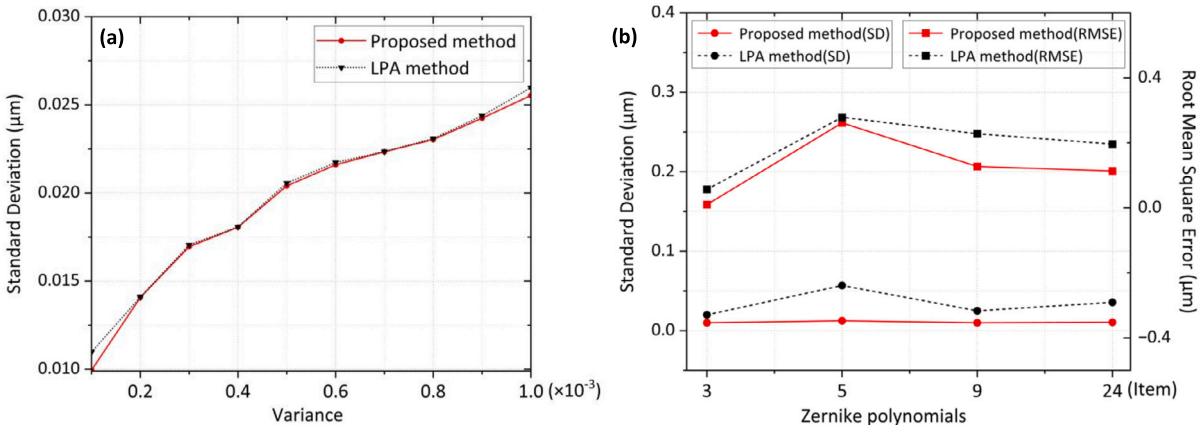

Fig. 3. The residue standard deviation (SD) and root mean square error (RMSE) curves of proposed method and LPA. (a) Comparison of SD between the proposed method and LPA under different noise variance. (b) Comparison of SD and RMSE between the proposed method and LPA under different aberrations.

evaluate the robustness against noise and accuracy improvement of the proposed algorithm, we performed the following simulation analyses. First, under the working condition of keeping tilt aberration, Gaussian-distributed random noise with variance varying uniformly from 10^{-4} to 10^{-3} were added to the simulated step sample respectively, to compare the topography restoration of the proposed approach and LPA. The noise intensity was selected to match the subsequent experimental conditions. The height map extracted by the proposed method and LPA is subtracted from the original topography to obtain the residual map, as shown in Fig. 2(d) and (f). We calculated the overall standard deviation (SD) of the residual map, as shown in Fig. 3(a). From Fig. 3(a), we can conclude that the proposed method is robust to noise of different variance sizes with SD values below 30 nm.

To verify the proposed method's effectiveness in removing various aberrations, we simulated several possible aberrations in the actual optical system, such as tilt (item 3), defocus (item 5), spherical (item 9). In order to take into consideration of the higher-order aberrations that may also be present in the optical system, the tertiary spherical (item 24) aberration was added. These distortions were gradually superimposed into the simulated sample while keeping the noise variance level at 5×10^{-4}. The same step was to obtain the residual map of the extracted height distribution. Then, we calculated the root mean square error (RMSE) and SD values of the residue to quantify the accuracy improvement of the proposed method, as shown in Fig. 3(b). The RMSE values of LPA were 56.78 nm, 278.79 nm, 227.9 nm and 196.4 nm, respectively, while the results of proposed method were 10.02 nm, 261.59 nm, 127.30 nm, and 113.60 nm for these four cases above, which are smaller than those obtained by LPA. The SD values of LPA were 20.03 nm, 56.78 nm, 25.13 nm and 35.73 nm, respectively, while the results of proposed method were 10.03 nm, 12.49 nm, 10.00 nm and 10.57 nm. The above cases show that both SD and RMSE values calculated by proposed method were smaller than those obtained by LPA. Meanwhile, it can be seen from Fig. 3(b) that the SD and RMSE values were highest when defocus is introduced to the sample. This is because the surface shape exhibits a dramatic concavity when defocus aberration is added. The shape of the sample was truncated by depressions and wrapped together, which affected the accuracy of phase unwrapping and aberration compensation. The above analysis illuminated that, while maintaining the same robustness against noise as LPA, the proposed method has significantly improved resistance to various aberrations, even in the case of complex high-order aberrations.

4. Experiment and results

The experiment was carried out in a DHM optical system to assess the performance of proposed method. Fig. 4(a) and (c) illustrates the experimental setup for a single-shot, off-axis, dual-wavelength DHM system. In order to separate the two reference beams angularly, laser beams with wavelengths of 532 nm (laser 1) and 561 nm (laser 2) were respectively tuned to horizontal and vertical polarization states using a polarizer. The modulated beams were subsequently collimated by a spatial filter (SF), expanding the beam by a factor of 10, and then split into object beam and reference beam via an unpolarized beam splitter (BS2). The reference light passed through a polarized beam splitter (PBS), with the 532 nm beam being completely reflected and the 561 nm beam being transmitted. The angle at which the two reference beams reached the camera target surface was adjusted using two mirrors (M3 and M4). The relevant schematic diagram is shown in Fig. 4(b). The off-axis angle between the object beam and reference beam was set by angular tilting of BS3, further improving space frequency utilization by adjusting its angle. A CCD camera was positioned on the imaging plane to capture the interference fringes of the dual-wavelength holograms. The camera operated with an exposure time of 150 μs, a full-width resolution of 560×560 pixels, and a pixel size of 3.45 μm. Finally, frequency distributions of the dual-wavelength holograms were obtained in the frequency domain, with the 532 nm and 561 nm holograms chosen respectively.

A periodic step sample, similar to the microgroove structures in MEMS, was measured to assess the performance of the proposed method. The performance of the proposed method was assessed by imaging and height characterizing of a standard step sample using the experimental system in Fig. 4. The height of step was 4 μm. Dual-wavelength holograms were obtained in a single-shot experiment. As shown in Fig. 5(a) and (b), the corresponding phase maps at the respective wavelengths were acquired through off-axis reconstruction. After layered aberration processing of the two phase maps (Fig. 5(d)), Fig. 5(c) shows the height maps obtained by the proposed method.

To quantitatively evaluate the performance optimization achieved by the proposed algorithm, we selected a cross-section (Fig. 5(e)) in the 3D shape distribution to plot the contour curves, as shown in Fig. 6. The black dashed line represents the contour curves obtained by LPA, while the red solid line represents those obtained by proposed method. As a standard result, we added the height distribution by commercial surface profiler (ZYGO) [30] on the charts. We selected 10 points uniformly for the contour curves of the step plane, calculating the SD and RMSE values. Notably, in the smooth area at the top of the step, bottom area of the step (9 ~ 11 μm), and the area of sharp rise in step height (11 ~ 13 μm), the height distribution obtained by LPA did not meet that of the sample, affecting the calculation of thickness. The proposed method significantly attenuated the distortion of the height distribution, resulting in a reduction of the SD in the step profile height from 177.34 nm to 66.29 nm. Meanwhile, the RMSE values had a reduction from 209.08 nm to 73.09 nm (Table 1). For the ROI region boxed out in Fig. 5, the PV val-

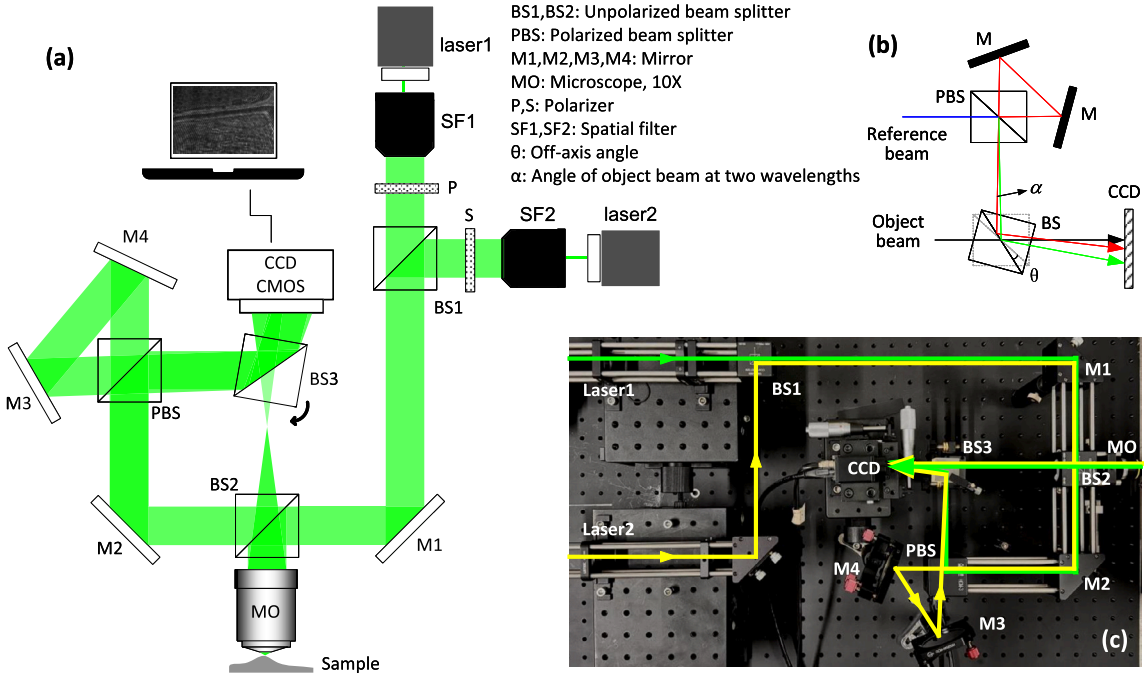

Fig. 4. Single-shot DW-DHM experiment system: (a), (c) are the optical system setup, (b) shows the realization of two reference beams separation.

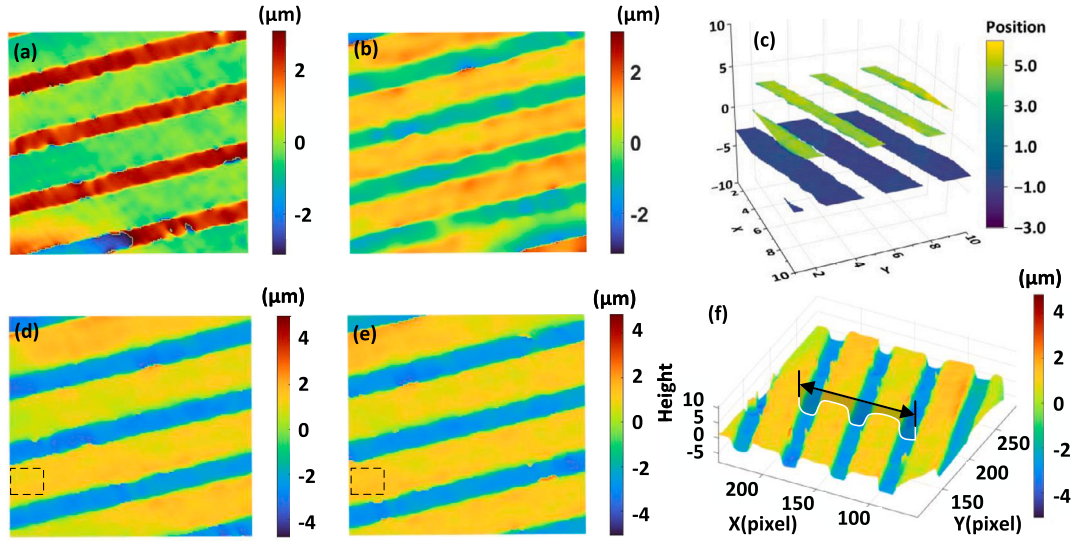

Fig. 5. The experimental results of standard step obtained with the proposed method and LPA: (a) Phase map of 561 nm. (b) Phase map of 532 nm. (c) Schematic diagram of layered processing. Height result with (d) LPA and (e)the proposed method.(f) 3D distribution of (e).

Table 1
Measurement data of standard step sample.

	SD (nm)	RMSE (nm)
LPA	177.34	209.08
Proposed method	66.29	73.09

ues were calculated and the results were 125.36 nm for LPA and 37.19 nm for the proposed method. This indicates that the proposed method computes a flatter surface shape compared to LPA. Therefore, the proposed method can significantly eliminate the aberration in complex step structures, effectively improving the problem that the results obtained by LPA are affected by phase aberration.

Finally, measurements were performed on a MEMS sample with step structure (height: 1 μm) to further validate the proposed method. The height distribution of the MEMS sample calculated by LPA and the proposed method were shown both in Figs. 7 and 8. As can be seen in Fig. 8, due to the effect of aberration, the height map and curve with LPA were distorted at the bottom and top surface, resulting in the average RMSE of 87.95 nm. However, the proposed method eliminated the effect of distortion very well, with the average RMSE of 36.90 nm. The above results demonstrate the good performance of the proposed method.

5. Conclusion

In summary, we developed a layered dual-wavelength phase restoration method to effectively mitigate system aberrations and distortions in phase reconstruction for high aspect ratio step structures. For a sample

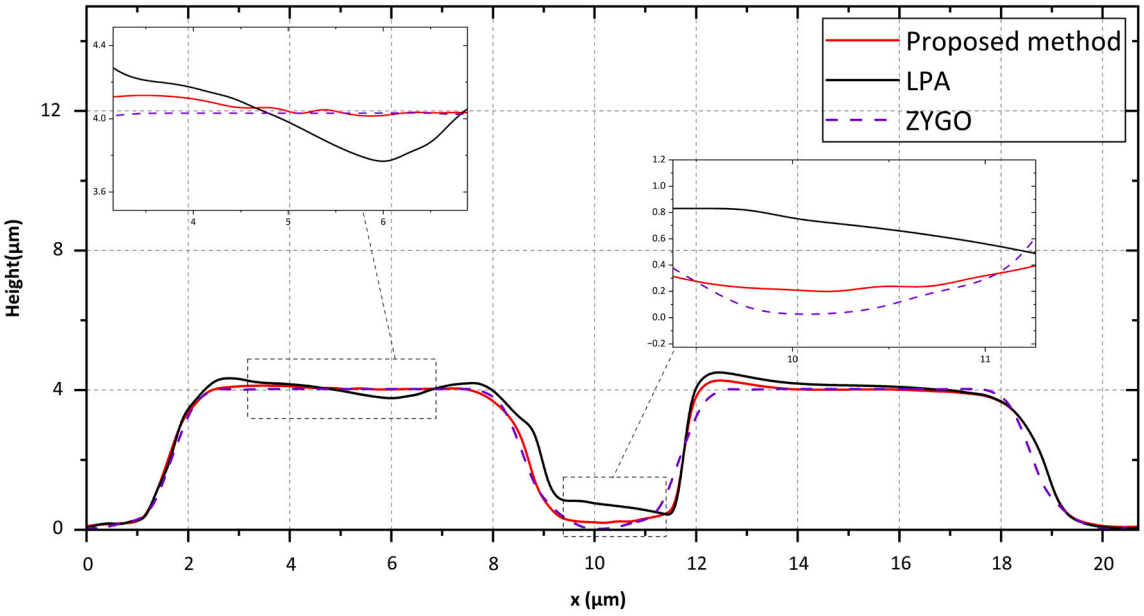

Fig. 6. Comparison of the profile curves of standard step sample calculated by LPA, proposed method and ZYGO surface profiler [30].

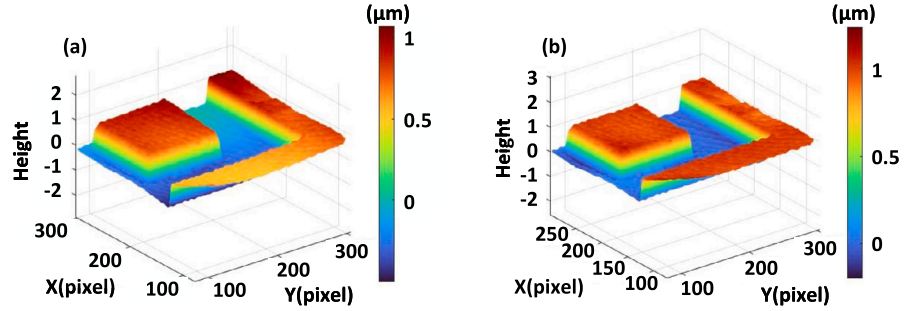

Fig. 7. Height maps of MEMS sample calculated by (a) LPA and (b) the proposed method.

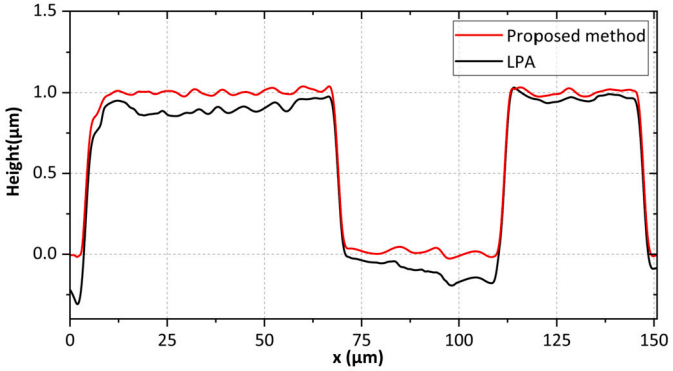

Fig. 8. Comparison of the profile curves of MEMS sample inverted by LPA and the proposed method.

with a height of 2 microns, we simulated the SD and RMSE of both the proposed layered dual-wavelength phase restoration method and LPA under various types of noise and aberration. The results demonstrate that, compared with LPA, the proposed approach offers substantial improvement in resisting distortions caused by tilt, defocus, and spherical aberrations in the optical system.

To further assess the method's performance, we conducted experiments using a DW-DHM optical system on a periodic step sample with a height of 4 microns, resembling the micro-groove structures found in MEMS. A dual-wavelength hologram was captured in a single experiment, and phase images were reconstructed at each wavelength using off-axis reconstruction. After applying layered aberration correction to the phase images, the resulting height map showed that the proposed method significantly reduced height distribution distortions compared to LPA. The standard deviation of the step profile height decreased from 177.34 nm to 66.29 nm, and the RMSE was reduced from 209.08 nm to 73.09 nm, confirming the effectiveness of the proposed method. A MEMS sample was measured and characterized. The RMSE was reduced from 87.95 nm to 36.90 nm, demonstrating the potential of the proposed method for application in the field of micro-nano structure device measurements.

Specifically, both numerical and experimental results demonstrate that, while maintaining the same robustness against noise as LPA, the proposed method effectively mitigates the amplification of dual-wavelength technique aberrations, phase restoration accuracy has been significantly improved. Consequently, it facilitates improved fidelity in reconstructing complex microstructural features. This method showcases considerable potential as a valuable tool for advancing precision imaging and micro-nano structures analysis.

CRediT authorship contribution statement

Yuxuan Zhao: Writing – original draft, Resources, Investigation. **Lei Zeng:** Investigation, Data curation. **Zhiming Lin:** Formal analysis. **Qiwen Jin:** Formal analysis, Data curation. **Yingchun Wu:** Writing – review & editing. **Chenghang Zheng:** Writing – review & editing. **Zhibin Wang:** Visualization. **Yongxin Zhang:** Visualization. **Xuecheng Wu:** Writing – review & editing, Visualization.

Declaration of competing interest

The authors declare that they have no known competing financial interests or personal relationships that could have appeared to influence the work reported in this paper.

Acknowledgement

The authors thank the National Natural Science Foundation of China (52276167), Zhejiang Provincial Natural Science Foundation of China (ZCLQ24E0601), the Fundamental Research Funds for the Central Universities (2022ZFJH004). We would also like to acknowledge inspiring discussions with Dr. Lyu.

Data availability

Data will be made available on request.

References

[1] Gabor D. A new microscopic principle; 1948.
[2] Charrière F, Kühn J, Colomb T, Montfort F, Cuche E, Emery Y, et al. Characterization of microlenses by digital holographic microscopy. Appl Opt 2006;45(5):829–35.
[3] Kreis T. Handbook of holographic interferometry: optical and digital methods. John Wiley & Sons; 2006.
[4] Parshall D, Kim MK. Digital holographic microscopy with dual-wavelength phase unwrapping. Appl Opt 2006;45(3):451–9.
[5] Kühn J, Colomb T, Montfort F, Charrière F, Emery Y, Cuche E, et al. Real-time dual-wavelength digital holographic microscopy with a single hologram acquisition. Opt Express 2007;15(12):7231–42.
[6] Michelson AA. Détermination expérimentale de la valeur du mètre en longueurs d'ondes lumineuses. Gauthier-Villars et fils; 1894.
[7] Wyant J. Testing aspherics using two-wavelength holography. Appl Opt 1971;10(9):2113–8.
[8] Guo R, Wang F. Compact and stable real-time dual-wavelength digital holographic microscopy with a long-working distance objective. Opt Express 2017;25(20):24512–20.
[9] Huang M, Qin H, Jiang Z. Real-time quantitative phase imaging by single-shot dual-wavelength off-axis digital holographic microscopy. Appl Opt 2021;60(15):4418–25.
[10] Ibrahim DGA. Dual-wavelength digital holographic microscope for accurate surface micro-topography measurement. In: Advanced solid state lasers. Optica Publishing Group; 2019. p. JTh3A–54.
[11] Zhang H, Hou S, Ma B, Cai P, Yang J, Yan H. 3d measurement of rough objects based on dual wavelength digital holography. In: International conference on optical and photonic engineering (icOPEN 2022), vol. 12550. SPIE; 2023. p. 214–9.
[12] Li X, Qin G, Zou Y, Yu W, Hu R, Qu J, et al. Dual-wavelength real-time simultaneous phase imaging based on off-axis interferometry. Opt Lasers Eng 2023;165:107565.
[13] Abdelsalam D, Magnusson R, Kim D. Single-shot, dual-wavelength digital holography based on polarizing separation. Appl Opt 2011;50(19):3360–8.
[14] Wu D, Xie L, Han X, Zhou C, Bu Z, Liu S, et al. Convenient dual-wavelength digital holography based on orthogonal polarization strategy with a wollaston prism. Appl Opt 2024;63(7):B70–5.
[15] Persano A, Tazzoli A, Farinelli P, Meneghesso G, Siciliano P, Quaranta F. K-band capacitive mems switches on gaas substrate: design, fabrication, and reliability. Microelectron Reliab 2012;52(9–10):2245–9.
[16] Payne JE, Nyholm P, Beazer R, Eddy J, Stevenson H, Ferguson B, et al. Fabrication of high aspect ratio, non-line-of-sight vias in silicon carbide by a two-photon absorption method. Sci Rep 2024;14(1):2176.
[17] Bogue R. Recent developments in mems sensors: a review of applications, markets and technologies. Sens Rev 2013;33(4):300–4.
[18] Zhou Haowen, Hussain Mallik MR, Banerjee Partha P. A review of the dual-wavelength technique for phase imaging and 3D topography. Light Adv Manuf 2022;3(2):314–34.
[19] Pagliarulo V, Miccio L, Ferraro P. Digital holographic microscopy for the characterization of microelectromechanical systems. In: Optical micro-and nanometrology VI, vol. 9890. SPIE; 2016. p. 989002.
[20] Williams L, Banerjee PP, Nehmetallah G, Praharaj S. Holographic volume displacement calculations via multiwavelength digital holography. Appl Opt 2014;53(8):1597–603.
[21] Liu W, Tao S, Cheng F, Yang Z, Wang W, Kong M. Phase compensation algorithm based on image segmentation in dual-wavelength holographic microscopy. Appl Opt 2023;62(21):5815–21.
[22] Khmaladze A, Matz RL, Zhang C, Wang T, Holl MMB, Chen Z. Dual-wavelength linear regression phase unwrapping in three-dimensional microscopic images of cancer cells. Opt Lett 2011;36(6):912–4.
[23] Wang Z, Jiao J, Qu W, Yang F, Li H, Tian A, et al. Linear programming phase unwrapping for dual-wavelength digital holography. Appl Opt 2017;56(3):424–33.
[24] Shan M, Liu L, Zhong Z, Liu B, Zhang Y. Improved phase reconstruction using linear programming for dual-wavelength digital holography. Opt Lasers Eng 2019;117:1–6.
[25] Shan M, Meng N, Yu L, Zhong Z, Xie Y, Liu B, et al. Accelerated high-quality dual-wavelength digital holography using direct-retrieved synthetic-phases. Opt Laser Technol 2023;161:109138.
[26] Emery Y, Colomb T, Cuche E. Metrology applications using off-axis digital holography microscopy. J Phys Photon 2021;3(3):034016.
[27] Asundi A. Digital holography for MEMS and microsystem metrology, vol. 7. Wiley Online Library; 2011.
[28] Doblas A, Sánchez-Ortiga E, Martínez-Corral M, Saavedra G, Garcia-Sucerquia J. Accurate single-shot quantitative phase imaging of biological specimens with telecentric digital holographic microscopy. J Biomed Opt 2014;19(4):046022.
[29] Fuerschbach K, Rolland JP, Thompson KP. Theory of aberration fields for general optical systems with freeform surfaces. Opt Express 2014;22(22):26585–606.
[30] Optical surface profiler | profilometer | newview™ 9000. https://www.zygo.com/Products/MetrologySystems/3DOpticalProfilers/NewView9000, 2024/6/18.